Inorganic Chemistry

Article

pubs.acs.org/IC

Local Structure and La L_1 and L_3-Edge XANES Spectra of Lanthanum Complex Oxides

Hiroyuki Asakura,[†] Tetsuya Shishido,*[,‡,§] Kentaro Teramura,[§,¶,∥] and Tsunehiro Tanaka*[,§,¶]

[†]Synchrotron Radiation Research Center, Nagoya University, Furo-cho, Chikusa, Nagoya 464-8603, Japan

[‡]Materials Chemistry Course, Faculty of Urban Environmental Sciences, Tokyo Metropolitan University, 1-1 minami-Osawa, Hachioji 192-0397, Tokyo Japan

[§]Elements Strategy Initiative for Catalysts and Batteries (ESICB), Kyoto University, Kyoto, 615-8520, Japan

[¶]Department of Molecular Engineering, Graduate School of Engineering, Kyoto University, Kyoto 615-8510, Japan

[∥]Precursory Research for Embryonic Science and Technology (PRESTO), Japan Science and Technology Agency (JST), 4-1-8 Honcho, Kawaguchi, Saitama 332-0012, Japan

Supporting Information

ABSTRACT: La L_1 and L_3-edge X-ray absorption near-edge structure (XANES) of various La oxides were classified according to the local configuration of La. We found a correlation between both of the areas of the pre-edge peaks of the La L_1-edge XANES spectra and the full width at half-maximum of white line of La L_3-edge XANES spectra and the local configuration of La. Theoretical calculation of the XANES spectra and local density of states reveals the difference of La L_1 and L_3-edge XANES spectra of various La compounds is related to the p−d hybridization of the unoccupied band and broadening of the d band of La induced by the difference of local configuration. In addition, simplified bond angle analysis parameters defined by the angles of the La atom and the two adjacent oxygen atoms are correlated to the pre-edge peak intensity of the La L_1-edge XANES spectra. These results indicate that quantitative analysis of La L_1 and L_3-edge XANES spectra could be an indicator of the local structure of La materials.

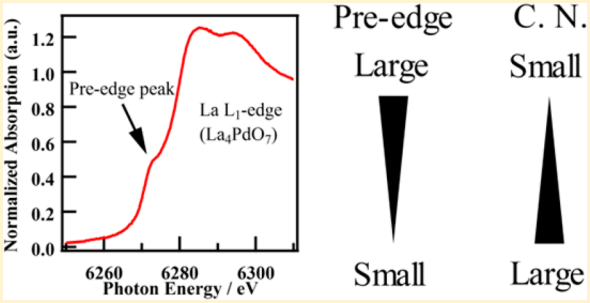

INTRODUCTION

Lanthanide is used in various fields such as magnetic material, dielectric material,[1] phosphor,[2] optical glass, hydrogen storage,[3] or catalysts because of its characteristic property derived from the unusual electronic configuration of 4f heavy electrons and the large ionic radii. For example, doping of La into $BaTiO_3$ has a strong influence on its dielectric property.[4−7] Yb^{3+}- and Nd^{3+}-doped Bi_2O_3−B_2O_3 glass works as low coherent wideband light sources.[8,9] In many cases, a small amount of lanthanide elements is added or doped into materials to develop or improve their characteristic property. The effects of the lanthanide additives depends on their location or electronic state in materials, but, in general, it is not easy to observe structural or chemical changes induced by a trace amount of such additives or structural or chemical information on such dopants themselves.

One of the widely used analytical techniques to clarify structural and chemical information on such trace elements is X-ray absorption spectroscopy (XAS). In particular, extended X-ray absorption fine structure (EXAFS), one part of XAS, has been already widely used in many fields including lanthanide materials. For example, the local structure of Er cation incorporated into glasses was studied by means of EXAFS,[10,11] and the authors estimated the disorder of oxygen atoms around Er, which could be related to the photoluminescence property. However, it is essentially difficult to construct a reliable model of the local structure of Er based on its EXAFS because of the disorder or amorphous nature of glass. X-ray absorption near edge structure (XANES), the other part of XAS, is also used to investigate coordination chemistry of lanthanide complexes[12−14] or to determine valence states of lanthanide compounds,[15,16] but the number of XANES applications of structural analysis is much smaller than the number of EXAFS applications. Our previous study of some of group V, VI, and VII metal (i.e., Nb, Mo, Ta, W, and Re) oxides indicated that the XANES spectra are subject to local configuration of the metals.[17,18] In the present study, La L_1 and L_3-edge XANES spectra of various La oxides were measured to find a relationship between the XANES spectra and their local structure. In addition, theoretical simulation of La L_1 and L_3-edge XANES spectra and local density of states (LDOS) were performed with FEFF code[19,20] to clarify the origin of the fine structure of the La L_1 and L_3-edge absorption edges.

Received: February 17, 2014
Published: May 29, 2014

dx.doi.org/10.1021/ic500381z | Inorg. Chem. 2014, 53, 6048−6053

EXPERIMENTAL SECTION

Sample Preparation of Lanthanum Oxides. Lanthanum complex oxides, La_4PdO_7, La_2CuO_4, $LaCuSrO_4$, $LaFeSrO_4$, $LaSrAlO_4$, $LaCoO_3$, and $LaAlO_3$ were prepared in solid-state reaction of vigorous grinding of precursors followed by high-temperature calcination. La_4PdO_7: La_2O_3 (325 mg, 1.0 mmol) and $Pd(OAc)_2$ (124 mg, 0.5 mmol); La_2CuO_4: La_2O_3 (652 mg, 2.0 mmol) and $Cu(OAc)_2$ (363 mg, 2.0 mmol); $LaCuSrO_4$: La_2O_3 (322 mg, 1.0 mmol), $Cu(OAc)_2$ (362 mg, 2.0 mmol), and $SrCO_3$ (295 mg, 2.0 mmol); $LaFeSrO_4$: La_2O_3 (325 mg, 1.0 mmol), $Fe(NO)_3{\cdot}9H_2O$ (810 mg, 2.0 mmol), and $SrCO_3$ (300 mg, 2.0 mmol); $LaSrAlO_4$: La_2O_3 (328 mg, 1.0 mmol), $SrCO_3$ (310 mg, 2.0 mmol), and $Al(NO)_3{\cdot}6H_2O$ (750 mg, 2.0 mmol); $LaCoO_3$: La_2O_3 (327 mg, 1.0 mmol) and $Co(NO_3)_2{\cdot}6H_2O$ (614 mg, 2.0 mmol); $LaAlO_3$: La_2O_3 (325 mg, 1.0 mmol) and $Al(NO)_3{\cdot}6H_2O$ (764 mg, 2.0 mmol). These mixtures were put into Al crucible and heated at 1423 K for 24 h. The identification was done by comparison of the XRD patterns of the prepared samples and those of the ones reported in literature.

XAS Measurement. La L_1 and L_3-edge XANES spectra of these materials were measured at the BL5S1, hard X-ray XAFS beamline, at Aichi Synchrotron Radiation Center[21] (AichiSR; Aichi Science and Technology Foundation, Aichi, Japan). The XANES spectra of their powder samples were recorded in transmission mode under ambient conditions, using a Si(111) double crystal monochromator. The photon energy was calibrated with the pre-edge peak (4966.0 eV) observed in the Ti K-edge XANES spectrum of Ti foil. Powder samples were mixed with an appropriate amount of boron nitride and pressed into pellets. Incident and transmitted X-ray fluxes were measured with ion chambers filled with He/N_2 (70/30%) and N_2/Ar (15/85%). Higher harmonic X-ray was cut off with proper glancing angle of Rh-coated collimating and focusing mirrors.

Data Reduction. A typical data reduction procedure (e.g., background removal, or normalization) was carried out with the Athena version 0.9.18 included in the Demeter package.[22] Curve-fitting analyses on the La L_1 and L_3-edge XANES spectra were also done with the peak-fitting function implemented into the Athena and the multipeak fitting procedure implemented in Igor Pro version 6.32 (Wavemetrics, Lake Oswego, OR, USA).

Theoretical Calculation. For the XANES and LDOS calculations, a structural model of each La oxides was constructed from the crystal structure reported in published literature with ATOMS package,[23] which contains all atoms within 10 Å around the target X-ray absorbing atom (La). If there were nonequivalent La sites, a structural model for each La site was constructed. We took into account not only electric dipole transition, but also electric quadrupole transition for the XANES simulation using the Hedin−Lundqvist function for the fine structure and ground state function for the background function (default setting for XANES calculation with FEFF) with self-consistent field (SCF) calculation and full multiple scattering (FMS). For the LDOS calculation, the Lorentzian broadening parameter was 1.0 eV.

RESULTS

Analysis of the Pre-Edge Peak Area of La L_1-edge XANES Spectra. Figure 1 shows the La L_1-edge XANES spectra of La_4PdO_7, La_2CuO_4, $LaCuSrO_4$, $LaFeSrO_4$, $LaSrAlO_4$, $LaCoO_3$, and $LaAlO_3$, with various local configuration around La^{3+} cation. The absorption edge of each compound is similar to each other, but the intensity of the characteristic pre-edge shoulder peaks at around 6275 eV varies among the samples. In the published literature,[24] the pre-edge peaks are assigned to electronic quadrupole transitions from 2s to 5d unoccupied states. $LaAlO_3$ and $LaCoO_3$, which have 12 adjacent oxygen atoms near the La atom, show the smallest shoulder peaks. $LaSrAlO_4$, $LaSrFeO_4$, and $LaSrCuO_4$, with nine nearest oxygen atoms, exhibit a bit more evident pre-edge peaks. Furthermore, La_4PdO_7 with seven-coordinated oxygen atoms and La_2CuO_4 bearing eight-coordinated oxygen atoms have the largest and

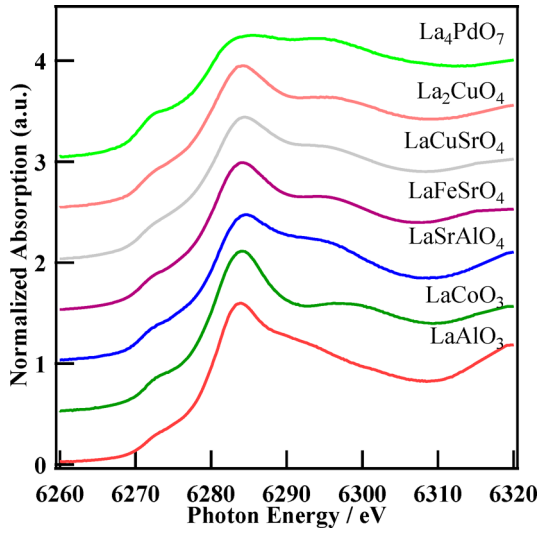

Figure 1. La L_1-edge XANES spectra of La_4PdO_7, La_2CuO_4, $LaCuSrO_4$, $LaFeSrO_4$, $LaSrAlO_4$, $LaCoO_3$, and $LaAlO_3$.

the second largest pre-edge peaks among the present La compounds. This indicates a possibility that the pre-edge peak area could be associated with some local configuration of La.

Thus, we performed curve fitting of the XANES spectrum with one Gaussian and one cubic function in a manner similar to that in the published literatures[25] to quantify the pre-edge peak area of each La L_1-edge XANES spectrum as an indicator of La local configuration. A result of the curve fitting of La L_1-edge XANES spectrum of La_2CuO_4 is shown in Figure 2.

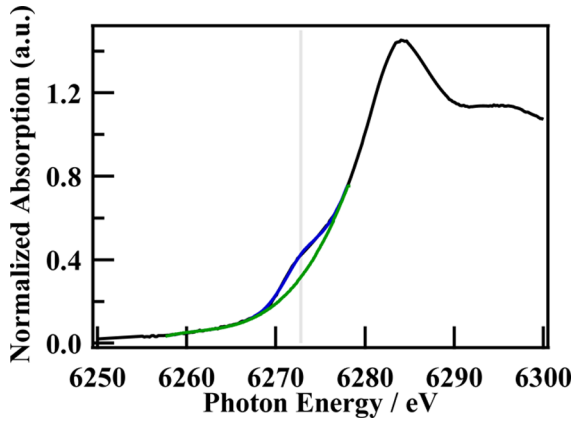

Figure 2. Curve-fitting of the pre-edge peak of La L_1-edge XANES spectrum of La_2CuO_4.

Clearly, one Gaussian and one cubic function are enough to fit the experimental data. The L_1-edge XANES spectra of the other La compounds were also successfully fitted in the same manner. The other curve-fitting results are provided in the Supporting Information.

Analysis of the White Line of La L_3-Edge XANES Spectra. Figure 3 shows the La L_3-edge XANES spectra of La_4PdO_7, La_2CuO_4, $LaCuSrO_4$, $LaFeSrO_4$, $LaSrAlO_4$, $LaCoO_3$, and $LaAlO_3$. All spectra exhibit one slightly asymmetric and strong white line at around 5490 eV. These peaks are assignable to electric transition from $2p_{3/2}$ to 5d state. $LaAlO_3$ and $LaCoO_3$, which have 12 adjacent oxygen atoms near the La^{3+} cation, show the narrowest white lines. $LaSrAlO_4$, $LaSrFeO_4$,

dx.doi.org/10.1021/ic500381z | Inorg. Chem. 2014, 53, 6048−6053

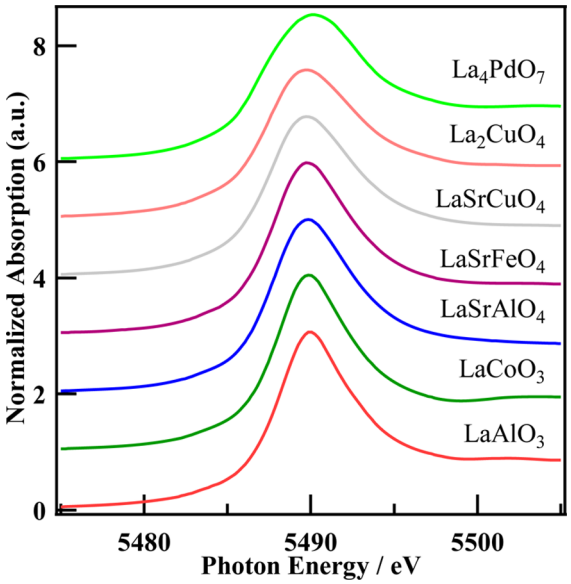

Figure 3. La L_3-edge XANES spectra of La_4PdO_7, La_2CuO_4, $LaCuSrO_4$, $LaFeSrO_4$, $LaSrAlO_4$, $LaCoO_3$, and $LaAlO_3$.

and $LaSrCuO_4$, with nine nearest oxygen atoms, exhibit slightly wider ones. Furthermore, La_4PdO_7 with seven-coordinated oxygen atoms and La_2CuO_4 bearing eight-coordinated oxygen atoms have the widest and the second widest white lines among the present La samples. Aritani et al. reported the width of white line of La_2O_3 is significantly larger than that of $La(OH)_3$ and pointed out that distortion of the local structure of the LaO_6 unit of La_2O_3 and $La(OH)_3$ could change the spectral shapes, qualitatively.[26] Similarly, the gradual change of the width of white line of La L_3-edge XANES spectra are assignable to the difference of the local configuration of LaO_x moiety.

We first calculated second derivatives of La L_3-edge XANES spectra to evaluate the d-orbital splitting depending on the local configuration of La in the same manner as our previous papers.[17,18] However, they were too noisy to quantify the difference of d-orbital broadening as shown in the Supporting Information. Thus, the full width at half-maximum (fwhm) of white line of each La L_3-edge XANES spectrum was estimated by curve analysis in a manner similar to that of the previous paper.[27] The La L_3-edge XANES spectrum was fitted with one arctangent function, which means the electric transition from $2p_{3/2}$ to continuum states, and one pseudo-Voigt function (Lorentzian/Gaussian = 1:1), which represents the transition to the unoccupied states. Figure 4 shows an example of peak-fitting analysis of La L_3-edge XANES spectrum of La_2CuO_4. The d-state broadening of the other La complex oxides were also estimated in the same manner (see Supporting Information) and discussed below.

Relationship between the Pre-Edge Peak Area of La L_1-Edge and the White Line fwhm of La L_3-Edge XANES Spectra. A clear correlation (R^2 = 0.95) between the pre-edge peak areas of La L_1-edge XANES spectra and the fwhm of the white line of L_3-edge XANES of La compounds is shown in Figure 5. This phenomenon is not unexpected because the pre-edge peak, which should be related to the mixing of p states into d states of La, and the d-state broadening must be induced by the change of the local configuration of La. Furthermore, there is an interesting relationship between the local structure and the electronic states observed by L_1 and L_3-edge XANES

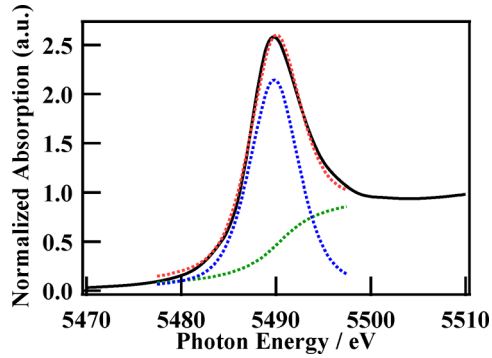

Figure 4. Peak fitting of the white line of La L_3-edge XANES spectrum of La_2CuO_4.

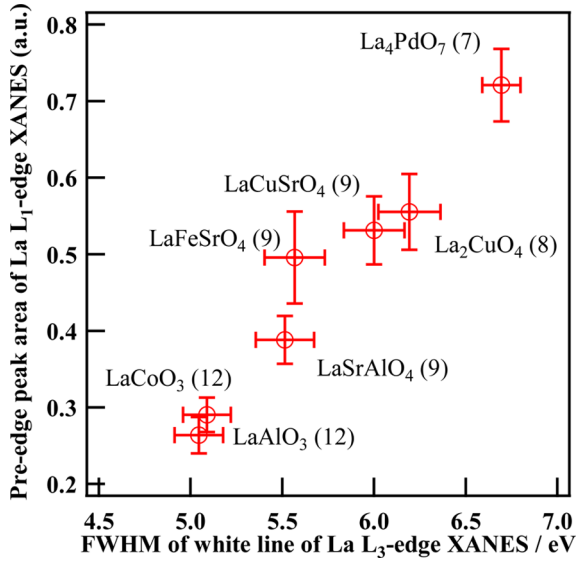

Figure 5. Dependence of pre-edge peak area of La L_1-edge XANES spectra on the fwhm of white line of La L_3-edge of La_4PdO_7, La_2CuO_4, $LaCuSrO_4$, $LaFeSrO_4$, $LaSrAlO_4$, $LaCoO_3$, and $LaAlO_3$. (The number in parentheses denotes the number of the coordinated oxygen atoms to La.)

spectra. That is, La_4PdO_7, which has a relatively small number of coordinated atoms to La, shows the largest pre-edge peak area and the widest fwhm of the white line in its L_3-edge XANES region, and, as the number of the adjacent atoms increases, the pre-edge peak intensity and the fwhm decrease.

Theoretical Calculation of L_1 and L_3-Edge La XANES Spectra and Local Density of States. The pre-edge peak of La L_1-edge XANES spectra and the difference of the fwhm of white line of La L_3-edge XANES spectra are temporarily interpreted into electric quadrupole transition from 2s to p−d hybridized unoccupied states and from $2p_{3/2}$ to 5d states, respectively. To clarify the origin of each feature observed at La L_1 and L_3-edge, theoretical calculation of L_1, L_3-edge XANES spectra and LDOS at La site were performed with FEFF 9.0 code.[20]

Figure 6 shows the La L_1 and L_3-edge XANES spectra and LDOS at La site of La_2CuO_4 calculated with FEFF 9.0. The energy axis for both of the L_1 and L_3-edge XANES spectra and LDOS is a relative value against the estimated Fermi level. The determination of the Fermi level with FEFF code is not so accurate, so the absolute value may be a little different from the true one, but it does not matter to discuss the origin of the pre-

dx.doi.org/10.1021/ic500381z | Inorg. Chem. 2014, 53, 6048−6053

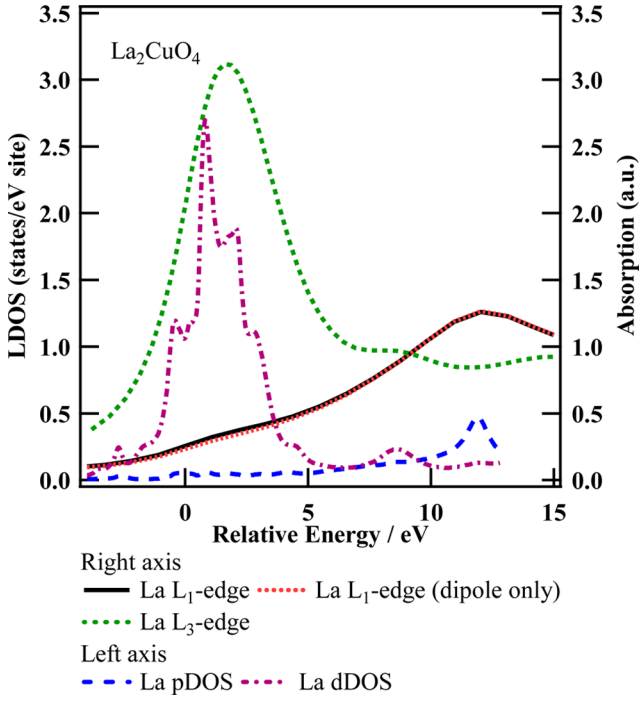

Figure 6. La L_1 and L_3-edge XANES spectra and LDOS at La site of La_2CuO_4 calculated with FEFF 9.0. (The relative energy is originated by the estimated Fermi energy.)

edge peak of the L_1-edge and white line of the L_3-edge. Clearly, the strong white line of La L_3-edge is ascribed to the unoccupied (mainly) d state. At the La L_1-edge, a small but distinct shoulder peak is observed at around 1 eV. Both of them are consistent with the discussion above.

In the published literature,[24] the pre-edge peak of the L_1-edge pre-edge is assumed to be electric dipole and quadrupole electronic transitions. However, the quadrupole transition is 2 orders of magnitude weaker than the dipole transition. As seen in Figure 6, both the electric dipole and the quadrupole transitions have distinct contributions, but the electric quadrupole transition is indeed significantly smaller than that of the dipole transition. To evaluate the contribution of quadrupole transition of La materials quantitatively, we also calculated the La L_1-edge XANES spectra of $LaAlO_3$ and La_4PdO_7.

In Figure 7, La L_1-edge XANES spectra of $LaAlO_3$, which shows the smallest pre-edge peak, and La_4PdO_7, which shows the largest pre-edge peak, calculated with only electric dipole

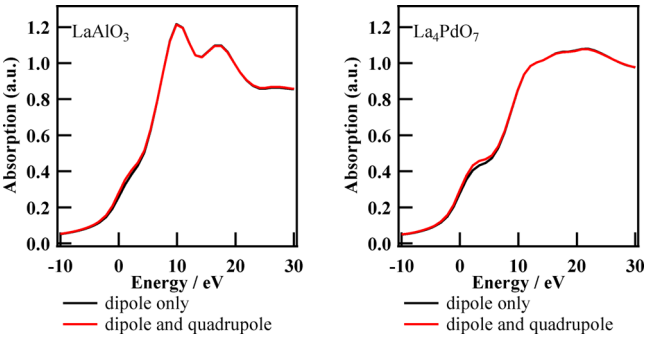

Figure 7. La L_1-edge XANES spectra of $LaAlO_3$ and La_4PdO_7 calculated with FEFF code with only electric dipole transition (black) and with both electric dipole and quadrupole transitions (red).

transition and with both of electric dipole and quadrupole transition are shown. The quadrupole transition has distinct but weak contribution to the pre-edge peak in both of them. The differential spectrum was also calculated for each spectrum, and we found the electric quadrupole contribution in these materials is almost the same. This means the quadrupole transition does not depend on the local structure of La, but the dipole transition depends on it. It is expected because the d character of the unoccupied state is similar to each other among the present La oxides, but p character ratio of the unoccupied state is altered by the local configuration of La. In addition, this indicates the pre-edge peak area extracted by curve fitting of L_1-edge XANES consists of an almost constant contribution of quadrupole transition and varying contribution of dipole transition affected by La surroundings.

Figure 8 shows a relationship between the pre-edge peak area of La L_1-edge XANES and p state contribution to the

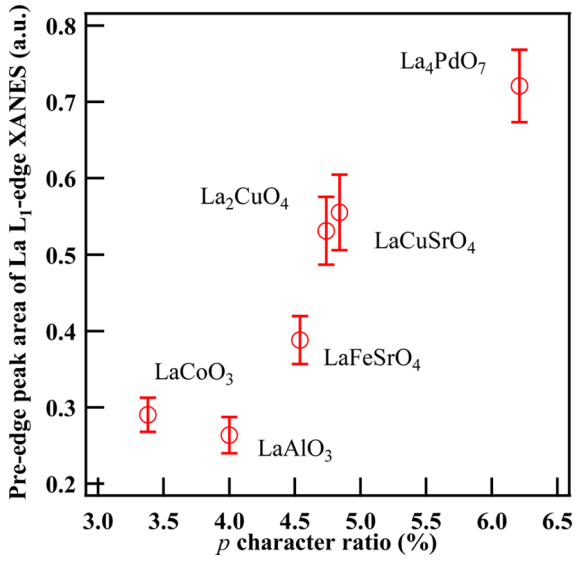

Figure 8. Dependence of pre-edge peak area of La L_1-edge XANES spectra on the p character ratio of LDOS around Fermi energy of La L_3-edge of La_4PdO_7, La_2CuO_4, $LaCuSrO_4$, $LaFeSrO_4$, $LaCoO_3$, and $LaAlO_3$.

unoccupied band. This correlation (R^2 = 0.87) also quantitatively demonstrates the pre-edge peak of L_1-edge XANES spectra is a probe for the p character of the unoccupied state, which is strongly related to the local configuration of La. For example, Roe et al. and Westre et al. have already reported similar analysis of the pre-edge peak of Fe K-edge XANES spectra of various Fe complexes, which are ascribed to the p−d hybridization of the unoccupied orbital in the final state. Roe et al.[28] used extended-Hückel calculation to evaluate the Fe 4p character in the final state to understand the difference of the pre-edge peak area of Fe K-edge XANES spectra and found a clear correlation between the pre-edge peak area and the 4p contribution ratio. Westre et al.[25] performed molecular orbital calculation of various Fe model molecules based on density functional theory in a similar manner, evaluated the contribution of each orbital by Mulliken population analysis, and clarified the relationships among the local symmetry, 4p character of the unoccupied orbitals, and the pre-edge peak structure of Fe K-edge XANES spectra. Yamazoe et al.[29] also reported a clear correlation among the energy gap of d orbital

dx.doi.org/10.1021/ic500381z | Inorg. Chem. 2014, 53, 6048−6053

splitting, the mixing ratio of 6p orbitals into 5d orbitals, and its local symmetry of various W model molecules.

Attempt of Parameterization of La Local Configuration and Its Relation to the XANES Spectra. In our previous paper[17,18] on the XANES spectra and the local structure of some of group V, VI, and VII metal (i.e., Nb, Mo, Ta, W, and Re) oxides, theoretical simulation of the electronic structure of minimal molecular models such as MO_4^{n-} or MO_6^{m-} (M stands for Nb, Mo, Ta, W, or Re, and n and m stand for appropriate numbers of additional electrons) indicated that change of the atomic distance between the X-ray absorbing atom (M) and adjacent oxygen atoms had little influence on the pre-edge peak intensity, but angular change of O−M−O strongly affected the pre-edge peak intensity. The centrosymmetry of the M cation strongly affects their XANES spectra. In the group V, VI, and VII elements, there are only four-, five-, and six-coordinated units such as lowly centrosymmetric tetrahedral WO_4 unit of highly centrosymmetric octahedral WO_6 unit, for example.

On the other hand, in the case of elements with very large ionic radii such as La, its oxides could be accompanied by 7 to 12 coordinated oxygen atoms. The centrosymmetry of La coordination sphere might be considered to be high with 12-coordinated atoms and low with seven-coordinated ones. In addition, atomic distance between La and coordinated atoms could also vary from about 2.0 to about 3.5 Å. As discussed on lanthanide-doped glass in the introduction, it is not easy to determine the local configuration of lanthanide atoms in amorphous materials with EXAFS spectroscopy. Thus, we tried to parametrize the local configuration of La and investigate the relationship between it and the corresponding XANES spectrum.

In the field of metallurgy, the degree of distortion or defect of the microstructure of every metal atom in bulk metal could be evaluated on various criteria in the terms of molecular dynamics[30] (MD). For example, the centrosymmetry parameter (CSP) is proposed by Kelchner et al.[31] to evaluate the defect or dislocation of metal. Ackland et al. used bond angle analysis (BAA) to identify the local coordination, distinguishing face-centered cubic, hexagonal close-packed, body-centered cubic, and other structures of each metal atom simulated by MD and so forth.[32] We applied the CSP and simplified BAA methods to parametrize the local configuration of the La center and found that a simplified BAA analysis could be used to produce well-correlated parameters to the characteristic features of the XANES spectra in the following procedure. Simplified BAA parameter is defined in the following equation, where n and θ_{ijk} denote the number of independent angles and the angle formed by the central atom j and two of its adjacent atoms i and k, respectively. If there are unidentical sites of La, the BAA parameter is calculated as an average value of each BAA parameter on each site.

$$\mathrm{BAA} = \frac{1}{n}\sum |\cos(\theta_{ijk})|$$

First, the Cartesian coordinates of the nearest adjacent oxygen atoms into the La located at the origin (0, 0, 0) are extracted from the crystal structure within 3.3 Å from La center. Second, the absolute values of cosine of every angle formed by La and two adjacent oxygen atoms are summed up and averaged by the number of independent angles. For example, the simplified BAA parameters of six-coordinated regular octahedron, eight-coordinated cube, and 12-coordinated icosahedron are 0.2, 0.429, and 0.455, respectively. Thus, the simplified BAA parameter increases as the coordination number increases at least in the range from 6 to 12.

The dependence of pre-edge peak area of La L_1-edge XANES spectra on the BAA parameters of La oxides is summarized in Figure 9. The pre-edge peak areas of L_1-edge XANES spectra

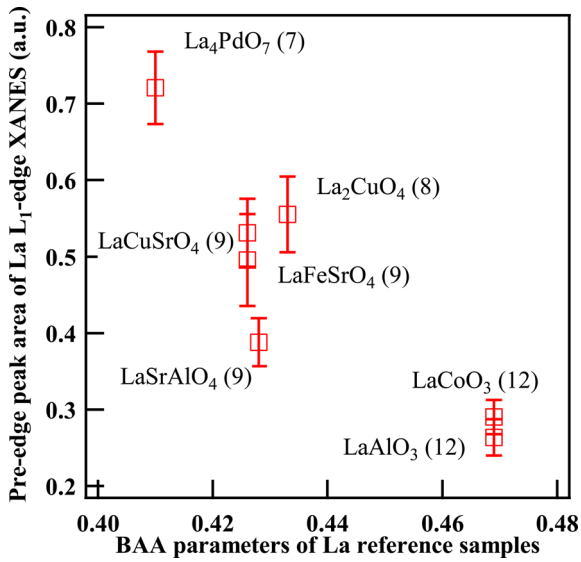

Figure 9. Dependence of pre-edge peak area of La L_1-edge XANES spectra on the BAA parameters of La_4PdO_7, La_2CuO_4, $LaCuSrO_4$, $LaFeSrO_4$, $LaSrAlO_4$, $LaCoO_3$, and $LaAlO_3$. (The number in parentheses denotes the number of the coordinated oxygen atoms to La.)

have a significant correlation (R^2 = 0.79) to the BAA parameters. This indicates the BAA parameter, which could be calculated from an arbitrary model, even an amorphous one, could be an indicator of the coordination number, or at least and indicator of the local configuration of La in the range from 7 to 12 of its coordination number. As mentioned above, the BAA parameter of the regular octahedron is 0.2, and it seems to be difficult to extend this simplified bond angle analysis into six-coordinated La materials.

This relationship also indicates that a combination of XANES measurement and MD simulation could open a way for structural analysis of amorphous materials. For example, one can simulate the distribution of a trace amount lanthanide atoms in a glass system with some MD code, but simulation of the XANES spectra of lanthanide atoms in such a system is generally very time-consuming because there are enormous numbers of lanthanide atoms in different local environments. The BAA parameters could be calculated easily from the simulated atomic distribution with MD simulation. If the calculated BAA parameters of considerable systems are significantly different from each other, it would be worth measuring their XANES spectra for semiquantitative analysis of lanthanide local configuration.

CONCLUSION

La L_1-edge and L_3-edge XANES spectra of various La compounds are summarized and found to have a good correlation with the La local structure. These results indicate that quantitative analysis on the L_1 and L_3-edge XANES spectra might give a piece of information on the local configuration of

dx.doi.org/10.1021/ic500381z | Inorg. Chem. 2014, 53, 6048−6053

trace lanthanide elements in optical glasses, catalysts, magnetic materials, and so on. This methodology might also give some insight into thermal vibration of lanthanides element in lanthanide complex materials such as skutterudites, for example. Theoretical simulation of La L_1 and L_3-edge XANES spectra and LDOS at La site of various La compounds supported the relationship between the local structure of La and its XANES spectrum. We also proposed primitive parameterization of the distortion of local structure of La. It is very primitive and empirical; it could not be directly linked to physical meanings at present, but it could be used to forecast whether XANES spectra could evaluate the local structure of the La elements of the target materials in the combination of XANES study and MD simulation or not. Further analysis on other lanthanides and real glass samples will be reported in near future.

■ ASSOCIATED CONTENT

Supporting Information

Curve-fitting analysis of La L_1-edge and La L_3-edge XANES spectra, second derivatives of La L_3-edge XANES spectra, differential spectra of calculated La L_1-edge XANES spectra. This material is available free of charge via the Internet at http://pubs.acs.org.

■ AUTHOR INFORMATION

Corresponding Authors

*E-mail: shishido-tetsuya@tmu.ac.jp (T.S.).
*E-mail: tanakat@moleng.kyoto-u.ac.jp (T.T.).

Notes

The authors declare no competing financial interest.

■ ACKNOWLEDGMENTS

This research is partially supported by the Adaptable and Seamless Technology Transfer Program through target-driven R&D (A-STEP, No. AS242Z02825M) by Japan Science and Technology Agency. The X-ray absorption experiments were performed under the approval of the Aichi Science and Technology Foundation (No. 2501004 and No. 2503010).

■ REFERENCES

(1) Park, H.-B.; Park, C. Y.; Hong, Y.-S.; Kim, K.; Kim, S.-J. *J. Am. Ceram. Soc.* **1999**, *82*, 94−102.
(2) Wakefield, G.; Holland, E.; Dobson, P. J.; Hutchison, J. L. *Adv. Mater.* **2001**, *13*, 1557−1560.
(3) Sakai, T.; Hazama, T.; Miyamura, H.; Kuriyama, N.; Kato, A.; Ishikawa, H. *J. Less-Common Met.* **1991**, *172*−*174* (Part 3), 1175−1184.
(4) Morrison, F. D.; Sinclair, D. C.; West, A. R. *J. Appl. Phys.* **1999**, *86*, 6355−6366.
(5) West, A. R.; Adams, T. B.; Morrison, F. D.; Sinclair, D. C. *J. Eur. Ceram. Soc.* **2004**, *24*, 1439−1448.
(6) Morrison, F. D.; Sinclair, D. C.; West, A. R. *J. Am. Ceram. Soc.* **2001**, *84*, 474−76.
(7) Morrison, F.; Coats, A.; Sinclair, D.; West, A. *J. Electroceram.* **2001**, *6*, 219−232.
(8) Fuchi, S.; Sakano, A.; Takeda, Y. *Jpn. J. Appl. Phys.* **2008**, *47*, 7932.
(9) Fuchi, S.; Sakano, A.; Mizutani, R.; Takeda, Y. *Glass Technology: Eur. J. Glass Sci. Technol., Part A* **2009**, *50*, 319−322.
(10) Marcus, M. A.; Polman, A. *J. Non-Cryst. Solids* **1991**, *136*, 260−265.
(11) Peters, P. M.; Houde-Walter, S. N. *J. Non-Cryst. Solids* **1998**, *239*, 162−169.
(12) Ellis, R. J.; Meridiano, Y.; Chiarizia, R.; Berthon, L.; Muller, J.; Couston, L.; Antonio, M. R. *Chem.—Eur. J.* **2013**, *19*, 2663−2675.
(13) Vitova, T.; Denecke, M. A.; Göttlicher, J.; Jorissen, K.; Kas, J. J.; Kvashnina, K.; Prüßmann, T.; Rehr, J. J.; Rothe, J. *J. Phys: Conf. Ser.* **2013**, *430*, 012117.
(14) D'Angelo, P.; Zitolo, A.; Migliorati, V.; Persson, I. *Chem.—Eur. J.* **2010**, *16*, 684−692.
(15) Hu, Z.; Kaindl, G.; Meyer, G. *J. Alloys Compd.* **1997**, *246*, 186−192.
(16) Yamamoto, T.; Yukumoto, A. *Bunseki Kagaku* **2013**, *62*, 555−563.
(17) Shishido, T.; Asakura, H.; Yamazoe, S.; Teramura, K.; Tanaka, T. *J. Phys: Conf. Ser.* **2009**, *190*, 012073.
(18) Asakura, H.; Shishido, T.; Yamazoe, S.; Teramura, K.; Tanaka, T. *J. Phys. Chem. C* **2011**, *115*, 23653−23663.
(19) Ankudinov, A. L.; Bouldin, C. E.; Rehr, J. J.; Sims, J.; Hung, H. *Phys. Rev. B* **2002**, *65*, 104107.
(20) Rehr, J. J.; Kas, J. J.; Vila, F. D.; Prange, M. P.; Jorissen, K. *Phys. Chem. Chem. Phys.* **2010**, *12*, 5503−5513.
(21) Tabuchi, M.; Asakura, H.; Takao, N.; Morimoto, H.; Watanabe, N.; Baba, Y.; Takeda, Y., *to be submitted*.
(22) Ravel, B.; Newville, M. *J. Synchrotron Radiat.* **2005**, *12*, 537−541.
(23) Ravel, B. *J. Synchrotron Radiat.* **2001**, *8*, 314−316.
(24) Larson, E. M.; Ellison, A. J. G.; Lytle, F. W.; Navrotsky, A.; Greegor, R. B.; Wong, J. *J. Non-Cryst. Solids* **1991**, *130*, 260−272.
(25) Westre, T. E.; Kennepohl, P.; DeWitt, J. G.; Hedman, B.; Hodgson, K. O.; Solomon, E. I. *J. Am. Chem. Soc.* **1997**, *119*, 6297−6314.
(26) Aritani, H.; Yamada, H.; Yamamoto, T.; Tanaka, T.; Imamura, S. *J. Synchrotron Radiat.* **2001**, *8*, 593−595.
(27) Rossetti, I.; Sordelli, L.; Ghigna, P.; Pin, S.; Scavini, M.; Forni, L. *Inorg. Chem.* **2011**, *50*, 3757−3765.
(28) Roe, A. L.; Schneider, D. J.; Mayer, R. J.; Pyrz, J. W.; Widom, J.; Que, L. *J. Am. Chem. Soc.* **1984**, *106*, 1676−1681.
(29) Yamazoe, S.; Hitomi, Y.; Shishido, T.; Tanaka, T. *J. Phys. Chem. C* **2008**, *112*, 6869−6879.
(30) Alexander, S. *Modell. Simul. Mater. Sci. Eng.* **2012**, *20*, 045021.
(31) Kelchner, C. L.; Plimpton, S. J.; Hamilton, J. C. *Phys. Rev. B* **1998**, *58*, 11085−11088.
(32) Ackland, G. J.; Jones, A. P. *Phys. Rev. B* **2006**, *73*, 054104.